could offer a possible explanation for the positive LOD scores in Family LD28.

Taking all the data into account, including an $\alpha$ estimate of 75 to 85% of LD families linked to chromosome 6q23-25, low conditional probability of linkage in 4 consanguineous families who lack homozygosities, sharing of 6q23-25 haplotypes by affected and unaffected individuals in these 4 families, and exclusionary LOD scores in 3 of these 4 families, one has to accept the possibility of another genetic locus in LD.

This study was supported by NIH grant NS21908 to Dr Delgado-Escueta, the DVA West Los Angeles Medical Center, The Hospital for Sick Children, Bloorview Children's Hospital Foundation, and the Lafora's Disease Associations of Quebec (Odette Malenfant) and Sweden (Vera Faludi).

We thank Dr Jacques Thibeault for providing the biopsies on Family LD28.

## References

1. Lafora GR. Uber das vorkommen amyloider korperchen im innern der ganglienzellen; zugleich ein beitrag zum studium der amyloiden substanz im nervensystem. Virchows Arch A Pathol Anat Histopathol 1911;205:295–303
2. Lafora GR, Glueck B. Contribution to the histopathology and pathogenesis of myoclonic epilepsy. Bull Gov Hosp Insane 1911;3:96
3. Harriman DGF, Millar JHD. Progressive familial myoclonic epilepsy in three families: its clinical features and pathological basis. Brain 1955;78:325–349
4. Schwarz GA, Yanoff M. Lafora's disease. Distinct clinicopathologic form of Unverricht's syndrome. Arch Neurol 1965;12: 172–188
5. Nishimura RN, Ishak KG, Reddick R, et al. Lafora disease: diagnosis by liver biopsy. Ann Neurol 1980;8:409–415
6. Carpenter S, Karpati G. Sweat gland duct cells in Lafora disease: diagnosis by skin biopsy. Neurology 1981;31:1564–1568
7. Busard HLSM, Gobreels-Festen AAWM, Renih WU, et al. Axilla skin biopsy; a reliable test for the diagnosis of Lafora's disease. Ann Neurol 1987;21:599–601
8. Van Heycop Ten Ham MW. Lafora disease, a form of progressive myoclonus epilepsy. Handbook of Clinical Neurology 1974;15:382–422
9. Roger J, Pellissier JF, Bureau M, et al. Le diagnostic précoce de la maladie de Lafora. Importance des manifestations paroxystiques visuelles et intérêt de la biopsie cutanée. Rev Neurol (Paris) 1983;139:115–124
10. Schwarz GA. Lafora's disease: a disorder of carbohydrate metabolism. In: Goldensohn ES, Appel SH, eds. Scientific approaches to clinical neurology. Philadelphia: Lea & Febiger, 1977:148–159
11. Serratosa JM, Delgado-Escueta AV, Posada I, et al. The gene for progressive myoclonus epilepsy of the Lafora type maps to chromosome 6q. Hum Mol Genet 1995;4:1657–1663
12. Sainz J, Minassian BA, Serratosa JM, et al. Lafora's progressive myoclonus epilepsy: narrowing the 6q24 locus by recombinations and homozygosities. Am J Hum Genet 1997;61:1205–1209
13. Minassian BA, Lee JR, Hherbrick JA, et al. Mutations in a gene encoding a novel protein tyrosine phosphatase cause progressive myoclonus epilepsy, Lafora type. Nat Genet 1998;20:171–174
14. Serratosa JM, Gomez-Garre P, Anta B, et al. A novel protein tyrosine phosphatase gene is mutated in progressive myodonus epilepsy of the Lafora type (EPM2). Hum Mol Genet 1999,8 (In press)
15. Weber JL, May PE. Abundant class of human DNA polymorphisms which can be typed using the polymerase chain reaction. Am J Hum Genet 1989;44:388–396
16. Lathrop GM, Lalouel JM, Julier C, Ott J. Multilocus linkage analysis in humans: detection of linkage and estimation of recombination. Am J Hum Genet 1985;37:482–498
17. Kruglyak L, Daly MJ, Reeve-Daly MP, Lander ES. Parametric and nonparametric linkage analysis: a unified multipoint approach. Am J Hum Genet 1996;58:1347–1363
18. Haldane JBS. The combination of linkage values and the calculation of distances between the loci of linked factors. J Genet 1919;8:299–309
19. Lander ES, Botstein D. Homozygosity mapping: a way to map human recessive traits with the DNA of inbred children. Science 1987;236:1567–1570

# Three-Dimensional Tracking of Axonal Projections in the Brain by Magnetic Resonance Imaging

Susumu Mori, PhD,* Barbara J. Crain, MD, PhD,† V. P. Chacko, PhD,* and Peter C. M. van Zijl, PhD*

**The relationship between brain structure and complex behavior is governed by large-scale neurocognitive networks. The availability of a noninvasive technique that can visualize the neuronal projections connecting the functional centers should therefore provide new keys to the understanding of brain function. By using high-resolution three-dimensional diffusion magnetic resonance imaging and a newly designed tracking approach, we show that neuronal pathways in the rat brain can be probed in situ. The results are validated through comparison with known anatomical locations of such fibers.**

Mori S, Crain BJ, Chacko VP, van Zijl PCM. Three-dimensional tracking of axonal projections in the brain by magnetic resonance imaging. Ann Neurol 1999;45:265–269

The white matter fibers in the brain are essential in linking functional regions. These neuronal projections have been traced in experimental animals, using invasive in vivo experiments,[1] but comparable human data

From the *Department of Radiology, Division of MRI Research, and †Department of Pathology, Johns Hopkins Medical School, Baltimore, MD.

Received Aug 17, 1998, and in revised form Oct 21. Accepted for publication Oct 23, 1998.

Address correspondence to Dr Mori, 217 Traylor, 720 Rutland Ave, Baltimore, MD 21205.

 

are necessarily much more limited. The availability of a noninvasive method for fiber tracking therefore would have a tremendous impact on our understanding of normal and abnormal brain function. Diffusion-weighted magnetic resonance imaging (MRI) allows in vivo mapping of the diffusional properties of brain water, and has revealed a high degree of diffusional anisotropy (directionality) in white matter.[2–11] Despite many studies of this anisotropy and the production of vector pictures showing fiber orientation within the volume elements (voxels) of image planes, the actual reconstruction of neuronal projections by tracking of these vectors has never been accomplished. In the present study, we demonstrate an approach called fiber assignment by continuous tracking (FACT), which is able to achieve such high-resolution three-dimensional (3D) tracking of axonal projections. The results are subsequently validated by in situ tracking of known fiber tracts in a rat brain.

## Materials and Methods

The principle of water-diffusion anisotropy is shown in Figure 1a. For a region where axons are aligned, water is restricted in the direction perpendicular to the axons and diffuses preferentially in a direction parallel to them. This situation can be represented mathematically by a so-called diffusion ellipsoid[5–11] (see Fig 1b), characterized by diffusion constants $\lambda_1$, $\lambda_2$, and $\lambda_3$ along its three orthogonal directions and the (vector) direction of the longest axis ($\lambda_1$). For example, $\lambda_1 \gg \lambda_2 = \lambda_3$ (anisotropic diffusion) suggests the existence of cylindrical structures preferentially aligned along $\lambda_1$, whereas $\lambda_1 = \lambda_2 = \lambda_3$ (isotropic diffusion) suggests sparse or unaligned axons. Although diffusion anisotropies have been detected previously in white matter, until now it has not been possible to translate these into neuronal trajectories. This problem is related to difficulties in the postprocessing reconstruction of 3D fiber structures from diffusion tensor MRI data, where decisions have to be made concerning the connections between voxels of the image. This is illustrated in Figure 1c, where the fibers (long curved arrows) are assumed to be confined to the two-dimensional (2D) plane and the fiber direction within each voxel is indicated by a straight open arrow. Starting from the voxel with an asterisk, tracking should follow the bold curved arrow. The most intuitive way to perform this tracking is by connecting each voxel to the adjacent one toward which the fiber direction is pointing. However, when using this approach, the tracking (indicated by the dotted voxels) often deviates from the true fiber orientation, because the choice of direction is limited to only eight angle ranges (26 in the case of 3D) (see Fig 1c). This problem is avoided when tracking a continuous rather than a discrete vector field (see Fig 1d). Here, tracking is initiated from the center of a voxel and proceeds according to the vector direction. At the point where the track leaves the voxel and enters the next, its direction is changed to that of the neighbor. Due to the presence of continuous intercepts, this tracking now connects the correct voxels and the actual fiber (bold straight arrows in Fig 1d) can be assigned. We therefore dubbed this approach FACT. The end point of the projection is judged based on the occurrence of sudden transitions in the fiber orientation (see Fig 1e and f). The severity of such a transition is quantified through a parameter *R*, presenting the summation of the inner products of nearby data points:

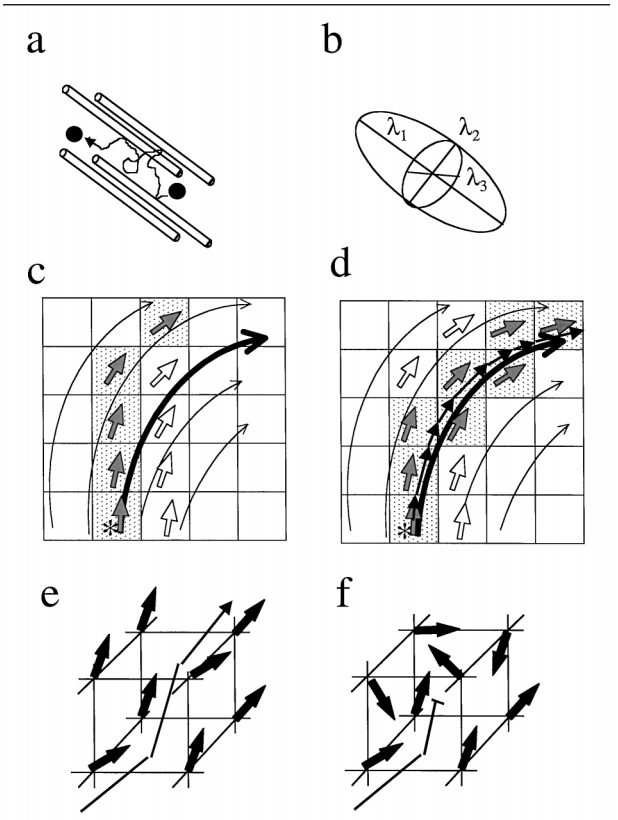


*Fig 1. Principle of fiber tracking. (a) Schematic view of restricted water diffusion (*solid sphere*) in an environment with strongly aligned fibers (depicted by bars). The diffusion properties can be fully described by an ellipsoid (b) with three principal axes ($\lambda_1$, $\lambda_2$, and $\lambda_3$) of which the orientation of the main axis represents the average fiber direction. Once this direction is determined in each voxel, tracking can be performed by using either a discrete (c) or a continuous (d) number field. The actual fibers are indicated by* curved arrows, *and the average fiber directions in the voxel are displayed as* open arrows. *The connected voxels resulting from tracking are shaded, using* dots. *The discrete approach leads to deviation from the actual fiber to be tracked (c), whereas the continuous approach succeeds as indicated by the train of* solid arrows *(d). A three-dimensional axonal projection can be tracked as long as nearby vectors are strongly aligned (e). When vector orientation becomes random, as judged quantitatively from summation of the inner products of these vectors (Eq 1), the tracking is ended (f).*

$$R = \sum_{i}^{s} \sum_{j}^{s} \mathrm{abs}(\nu_{\lambda 1i} \cdot \nu_{\lambda 1j})/s(s-1) \qquad (1)$$

where $\nu_{\lambda 1}$ is the unit vector representing the longest principal diffusion axis ($\lambda_1$) and $s$ is the number of data points

referenced. When adjacent fibers are aligned strongly (see Fig 1e), the $R$ value is large, while it becomes small (see Fig 1f) in regions without continuity in fiber direction. Theoretically, there are many ways to modify this criterion. In the present study, we calculated $R$ values by using the four neighboring voxels closest with respect to the continuous tracking position, and a fiber was judged discontinued for $R < 0.8$. The procedure of mapping the neuronal connections is started through the input of an arbitrary point in 3D space, after which the extent of the axonal projections into functional regions is traced in both the orthograde (forward) and the retrograde (backward) directions.

Studies were performed on a 400 MHz GE Omega (9.4 T), using a field of view of $32 \times 16 \times 16$ mm and $128 \times 64 \times 64$ data points zero-filled to a final resolution of $256 \times 128 \times 128$. Diffusion images were recorded by using a spin-echo Stejskal-Tanner sequence (echo time [TE] = 44 msec) and 10 gradient orientations. Gradient strength and length were 16 G/cm and 5 msec, with a separation of 16 msec. For an additional image with low diffusion weighting, a strength of 5 G/cm was used in the *xyz* direction. Diffusion tensor elements at each voxel were determined by multivariant least-square fitting weighted by signal-to-noise ratio.[12] The tensors were diagonalized to obtain $\lambda_1$, $\lambda_2$, and $\lambda_3$ and the direction of $\lambda_1$. The brain sample was obtained from an adult Sprague–Dawley rat and fixed on 5% formalin for 2 weeks.

## Results

Figure 2a shows a 2D representation of the water-diffusion measurements. Although existence of axonal projections can be clearly appreciated from this 2D vector picture, tracing of neuronal projections through the brain requires a complete 3D analysis. After extending the diffusion MRI into 3D, we applied the FACT analysis to track 10 different pathways in a formalin-fixed rat brain (Fig 3; see Fig 2b). It can be seen that our method successfully reconstructs the well-known structure of these projections. To further illustrate the validity of our approach, the tracking of the anterior commissure is also shown in a series of 2D planes and compared with the corresponding rat brain atlas from Paxinos and Watson[13] (see Fig 3d–f). The U shape of this structure can be easily appreciated from the atlas and it can be clearly seen that our diffusion result (dark blue) accurately traces this projection. These 2D slices also show part of the tracking of olfactory tract (ol), middle forebrain bundle (mfb), and fornix (f).

One interesting aspect of Figure 2a is the demonstration of aligned fibers in most areas of gray matter. Such anisotropy of gray matter has been reported previously, using diffusion measurements in two spatial orientations,[14] and our results extend on this earlier finding by showing the ordered fiber structures that cause the anisotropy.

## Discussion

Our results from using the FACT approach show that it is now possible to track the 3D structure of axonal projections by using the diffusion MRI technique. Although this is very promising, some limitations should be pointed out. First, MRI can only give information on the average axonal orientation within a voxel. Therefore, it is resolution dependent and it cannot distinguish among several very small projections that are immediately adjacent to each other. Second, the tracking method is unable to distinguish between afferent and efferent fibers. Further problems may occur if portions of two pathways actually touch, because the program may inadvertently switch pathways. For example, the initial tracking of the optic tract was complicated when reaching the level of the dorsal lateral geniculate, where the algorithm began a partial tracking of adjacent fimbrial axons. Other limitations are functions of the current algorithm. For example, one of the most challenging problems is the tracking of branched axons or axons leaving major pathways as they approach their targets. Our program traces only one of the branches in such a situation. An example is the tracking of the lateral olfactory tract (see Fig 3) for which the anterior portion is quite faithfully followed (see arrow in Fig 3d and e), but where the fibers that are actually identified in Figure 3f are small branches into olfactory and piriform cortex (indicated by dotted lines in the atlases of Fig 3d–f). As a result, the lateral olfactory tract itself, the location of which is still visible in the T2-weighted MRI scan (see arrow in Fig 3f), is not labeled at this level. Possible solutions to this problem depend on the specific question. For instance, if the goal is to follow various components of a pathway to their end points, one might simply identify multiple points in a large fiber bundle and track each component separately.

In summary, we introduced a 3D tracking method for diffusion MRI that allows the successful identification of axonal projections. Potential applications of this method include the study of neuronal development and of diseases affecting neuronal integrity. In the present study, a total of 12 hours were needed for the completion of the study. This time period can be easily shortened by a factor of 8 to 32 by using multiple-echo acquisition techniques.[15–17] Combined with recent methodological advances for the suppression of motion-related artifacts,[18–20] we expect clinical application of this fiber-reconstruction technique to be feasible in the near future.

This research was funded in part by a grant from Johns Hopkins School of Medicine, the American Federation of Aging Research, and the Whitaker Foundation.

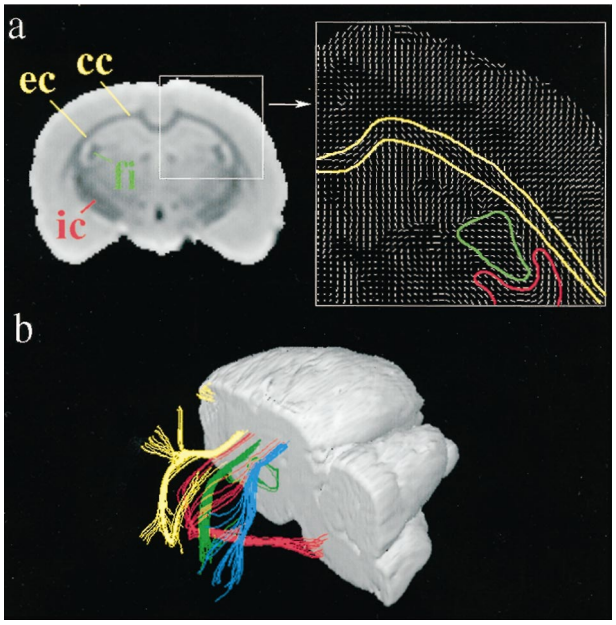


*Fig 2. Two-dimensional (2D) and three-dimensional (3D) tracking of prominent axonal projections. (a) 2D vector field presentation in the parietal lobe of a rat brain as localized from a section of the $T_2$-weighted magnetic resonance imaging scan. Because axonal orientations are projected onto the 2D plane, axons perpendicular to the plane appear as* dots. *Rough boundaries for regions of prominent fiber bundles are indicated by color lines (yellow = corpus callosum [*cc*] and external capsule [*ec*]; green = fimbria [*fi*]; and red = internal capsule [*ic*]. Notice the presence of preferential axonal orientation in the gray matter. (b) 3D presentation of the fibers. Color coding is the same as in (a) except for the blue color that shows axons tracked from the splenium of corpus callosum into the external capsule. Some axons within the fimbria are tracked into ventral hippocampal commissure, and axons within the internal capsule are tracked into the corpus callosum.*

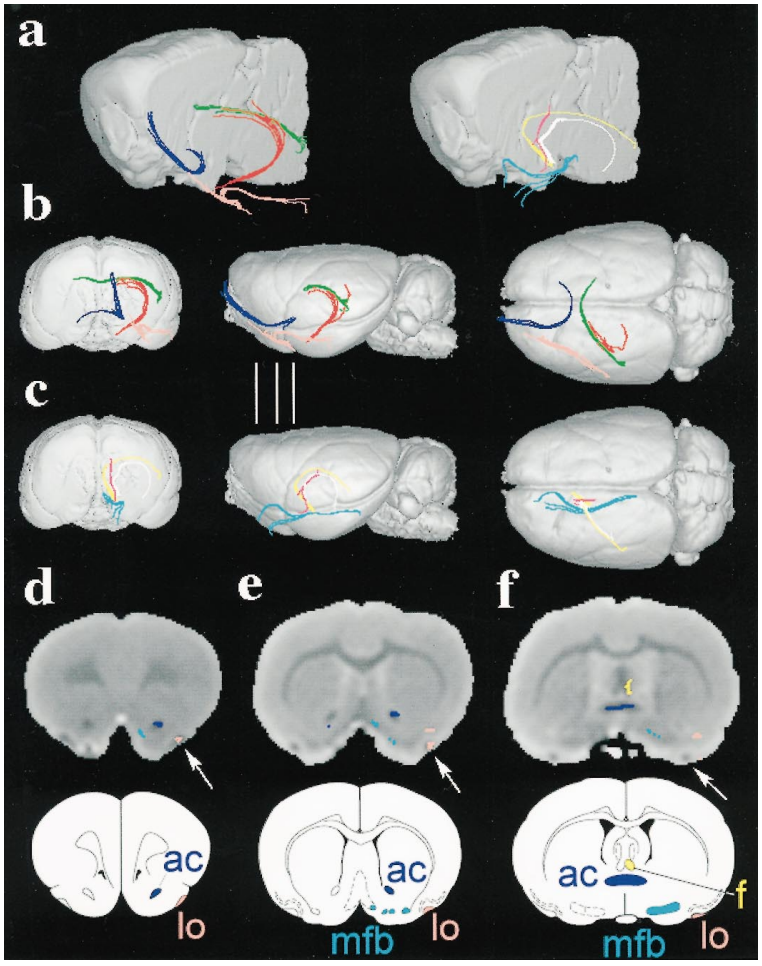


*Fig 3. Three-dimensional (3D) projections and two-dimensional (2D) validation of eight fiber bundles in the rat brain. The results of the tracking are superimposed on 3D volume images, using an oblique angle (a) or three orthogonal angles (b and c). The vertical lines between (b) and (c) indicate the positions of the 2D axial slices of $T_2$-weighted images on which the position of the tracking is superimposed (d–f). Images from the rat brain atlas[13] corresponding to the three slices in (d–f) are shown in the bottom row. Color codes are as follows: green = fimbria; dark blue = anterior commissure (*ac*); light blue = medial forebrain bundle (*mfb*); yellow = fornix (*f*); white = stria terminalis; pink = stria medullaris; red = optic tract; peach = lateral olfactory tract (*ol*).*

## References


1. Heimer L, Robards MJ. Neuroanatomical tract-tracing methods. New York: Plenum Press, 1981
2. Chenevert TL, Brunberg JA, Pipe JG. Anisotropic diffusion in human white matter: demonstration with MR technique in vivo. Radiology 1990;177:401–405
3. Moseley ME, Cohen Y, Kudarczyk J, et al. Diffusion-weighted MR imaging of anisotropic water diffusion in cat central nervous system. Radiology 1990;176:439–445
4. Moonen CTW, Prkar J, de Vleeschouner MH, et al. Restricted and anisotropic displacement of water in healthy cat brain and in stroke studied by NMR diffusion imaging. Magn Reson Med 1991;19:322–327
5. Basser PJ, Mattiello J, Le Bihan D. MR diffusion tensor spectroscopy and imaging. Biophys J 1994;66:259–267
6. Hsu EW, Mori S. Analytical interpretations of NMR diffusion measurements in an anisotropic medium and a simplified method for determining fiber orientation. Magn Reson Med 1995;34:194–200
7. Pierpaoli C, Jezzard P, Basser PJ, et al. Diffusion tensor MR imaging of human brain. Radiology 1996;201:637–648
8. Ulug AM, Bakht O, Bryan RN, van Zijl PCM. Mapping of human brain fibers using diffusion tensor imaging. In: Proceedings of the International Society for Magnetic Resonance in Medicine. 1325 New York: 1996:1325
9. Nakada T, Matsuzawa H. Three-dimensional anisotropy contrast magnetic resonance imaging of the rat nervous system: MR axonography. Neurosci Res 1995;22:389–398
10. Makris N, Worth AJ, Sorensen AG, et al. Morphometry of in vivo human white matter association pathways with diffusion weighted magnetic resonance imaging. Ann Neurol 1997;42: 951–962
11. Conturo TE, McKinstry RC, Aronovitz JA, Neil JJ. Diffusion MRI: precision, accuracy and flow effects. NMR Biomed 1995; 8:307–332
12. Basser PJ, Mattiello J, LeBihan D. Estimation of the effective self-diffusion tensor from the NMR spin echo. J Magn Reson B 1994;103:247–254
13. Paxinos G, Watson C. The rat brain in stereotaxic coordinates, 4th ed. San Diego: Academic Press, 1998
14. Thornton JS, et al. Anisotropic water diffusion in white and gray matter on the neonatal piglet brain before and after transient hypoxia-ischaemia. Magn Res Imaging 1997;15:433–440
15. Mansfield P. Multi-planar image formation using NMR spin-echoes. J Phys 1977;C10:L55–L58
16. Hennig J, Nauerth A, Friedburg H. RARE imaging: a fast imaging method for clinical MR. Magn Reson Med 1986;3:823–833
17. Beaulieu CF, Zhou X, Cofer GP, Johnson GA. Diffusion-weighted MR microscopy with fast spin-echo. Magn Reson Med 1993;30:201–206
18. Ordidge RJ, Helpern JA, Qing ZX, et al. Correction of motional artifacts in diffusion-weighted NMR images using navigator echoes. Magn Reson Imaging 1994;12:455–460
19. Anderson AW, Gore JC. Analysis and correction of motion artifacts in diffusion weighted imaging. Magn Reson Med 1994; 32:379–387
20. Mori S, van Zijl PCM. A motion correction scheme by twin-echo navigation for diffusion weighted magnetic resonance imaging with multiple RF echo acquisition. Magn Reson Med 1998;40:511–516


---

## Correction

The abstract by Yamasaki and colleagues that appeared in the September issue (Ann Neurol 1998;44:490–491) and the program of the American Neurological Association's 123rd Annual Meeting (pp 76–77) contained an error of copy editing that distorted its meaning. The full text of the corrected abstract appears here:

### T193. A Protein Critical for Immune-Mediated Demyelinating Disease

*Kenji Yamasaki, G. D. Ghadge, and R. P. Roos; Chicago, IL*

DA and other members of the TO subgroup of Theiler's murine encephalomyelitis virus persistently infect mice and cause a chronic demyelinating disease that resembles multiple sclerosis. Both diseases have a similar pathology, and in both the immune system plays a role in pathogenesis. In contrast, members of a GDVII subgroup produce an acute fatal encephalomyelitis and do not persist. We previously reported that demyelinating (but not nondemyelinating) strains have an initiation codon for translation for a protein (L*) out of frame with the viral polyprotein; mutant DA virus that does not have the L* initiation codon fails to induce a persistent infection or demyelination. These data suggest that L* is critically important for viral persistence and demyelination. To further test the role of L* in demyelinating disease, we have now engineered the GDVII viral genome to contain the L* initiation codon and to synthesize L*. The efficiency of expression of L* in mutant GDVII depends on particular nucleotides in an RNA stem loop structure near the L* initiation codon. Mutant GDVII virus that synthesizes L* is no longer neurovirulent. The presence of demyelination and virus persistence in survivors is under study.

Study supported by the National Multiple Sclerosis Society.

The publisher apologizes for the error.